Hyperpolarization-activated cation channels in fast-spiking interneurons of rat hippocampus

Yexica Aponte, Cheng-Chang Lien, Ellen Reisinger and Peter Jonas

J. Physiol. 2006;574;229-243; originally published online May 11, 2006;

DOI: 10.1113/jphysiol.2005.104042

Hyperpolarization-activated cation channels in fast-spiking interneurons of rat hippocampus

Yexica Aponte, Cheng-Chang Lien, Ellen Reisinger and Peter Jonas

Physiologisches Institut der Universität Freiburg, Hermann-Herder-Str. 7, D-79104 Freiburg, Germany

Hyperpolarization-activated channels (I_h or HCN channels) are widely expressed in principal neurons in the central nervous system. However, I_h in inhibitory GABAergic interneurons is less well characterized. We examined the functional properties of I_h in fast-spiking basket cells (BCs) of the dentate gyrus, using hippocampal slices from 17- to 21-day-old rats. Bath application of the I_h channel blocker ZD 7288 at a concentration of 30 μM induced a hyperpolarization of 5.7 ± 1.5 mV, an increase in input resistance and a correlated increase in apparent membrane time constant. ZD 7288 blocked a hyperpolarization-activated current in a concentration-dependent manner (IC_{50}, 1.4 μM). The effects of ZD 7288 were mimicked by external Cs^+. The reversal potential of I_h was −27.4 mV, corresponding to a Na^+ to K^+ permeability ratio (P_{Na}/P_K) of 0.36. The midpoint potential of the activation curve of I_h was −83.9 mV, and the activation time constant at −120 mV was 190 ms. Single-cell expression analysis using reverse transcription followed by quantitative polymerase chain reaction revealed that BCs coexpress HCN1 and HCN2 subunit mRNA, suggesting the formation of heteromeric HCN1/2 channels. ZD 7288 increased the current threshold for evoking antidromic action potentials by extracellular stimulation, consistent with the expression of I_h in BC axons. Finally, ZD 7288 decreased the frequency of miniature inhibitory postsynaptic currents (mIPSCs) in hippocampal granule cells, the main target cells of BCs, to 70 ± 4% of the control value. In contrast, the amplitude of mIPSCs was unchanged, consistent with the presence of I_h in inhibitory terminals. In conclusion, our results suggest that I_h channels are expressed in the somatodendritic region, axon and presynaptic elements of fast-spiking BCs in the hippocampus.

(Received 20 December 2005; accepted after revision 5 May 2006; first published online 11 May 2006)
Corresponding author P. Jonas: Physiologisches Institut, Universität Freiburg, Hermann-Herder-Str. 7, D-79104 Freiburg, Germany. Email: peter.jonas@physiologie.uni-freiburg.de

Among all GABAergic interneurons in the brain, interneurons of the basket cell (BC) subtype play a key role in network function. These interneurons are distinguished from other types of neurons by their fast-spiking action potential (AP) phenotype (Rudy & McBain, 2001), the expression of the Ca^{2+}-binding protein parvalbumin (Freund & Buzsáki, 1996) and the selective innervation of target cells in the perisomatic region (Buhl *et al.* 1994). BCs control both the number of active pyramidal cells and their AP frequency by feedforward and feedback inhibition (Pouille & Scanziani, 2004). BCs also control the timing of principal cell discharge, enabling temporal encoding in the brain. Finally, BCs play a pivotal role in the generation of synchrony and network oscillations (Buzsáki & Draguhn, 2004).

BCs are fast signalling devices with highly specialized membrane properties (Jonas *et al.* 2004). BCs show fast excitatory postsynaptic potentials and currents, mediated by rapidly gated AMPA-type glutamate receptors (Geiger *et al.* 1997). BCs generate APs at frequencies of several hundred Hertz under physiological conditions, as a result of the expression of voltage-gated Na^+ channels with rapid recovery from inactivation (Martina & Jonas, 1997) and voltage-gated K^+ channels with high activation threshold and rapid deactivation (Martina *et al.* 1998). Finally, BCs show a relatively positive resting potential, a low input resistance and a fast apparent membrane time constant (Geiger *et al.* 1997; Mott *et al.* 1997; Lübke *et al.* 1998; Jonas *et al.* 2004). While the positive resting potential sets the BCs into a ready-to-fire mode near the AP threshold from which excitatory inputs can efficiently trigger APs (Fricker *et al.* 1999), the fast apparent membrane time constant leads to a brief duration of excitatory postsynaptic potentials (EPSPs), allowing BCs to selectively respond to coincident principal neuron activity (Geiger *et al.* 1997).

Although the passive membrane properties are key determinants of synaptic integration and the input–output relation of fast-spiking BCs, the molecular basis is poorly understood. In the simplest possible scenario, resting potential and input resistance of a cell are determined

 DOI: 10.1113/jphysiol.2005.104042

by a single conductance. Primary candidates for such a conductance would be inwardly rectifying K^+ channels or two-pore domain K^+ channels (Goldstein *et al.* 2001). However, both types of channels are highly K^+-selective and thus cannot explain the combination of depolarized resting potential and low input resistance. Alternatively, resting potential and input resistance could be determined by the opposing actions of K^+-selective conductances and the non-selective cation conductance I_h, as recently proposed for cortical pyramidal neurons (Day *et al.* 2005; reviewed by Pape, 1996; Robinson & Siegelbaum, 2003). I_h channels are assembled from four subunits (HCN1–HCN4), which are abundantly expressed in the central nervous system (Pape, 1996; Gauss *et al.* 1998; Ludwig *et al.* 1998; Santoro *et al.* 1998, 2000; Magee, 1999; Williams & Stuart, 2000; Vasilyev & Barish, 2002). Functional studies indicate that I_h is expressed in hippocampal dendrite-inhibitory interneurons (Maccaferri & McBain, 1996; Lupica *et al.* 2001). Furthermore, immunocytochemical analysis revealed that HCN1–4 subunits are present in axons and presynaptic terminals of GABAergic interneurons in the hippocampus (Notomi & Shigemoto, 2004). However, unlike dendrite-inhibitory interneurons (Maccaferri & McBain, 1996; Lupica *et al.* 2001), BCs do not show an obvious 'sag' during hyperpolarizing current injection (Lübke *et al.* 1998), which argues against the expression of I_h. Thus, whether fast-spiking BCs express I_h has remained unknown.

In addition to setting resting potential and input resistance, several alternative functions of I_h have been suggested. First, I_h could contribute to the afterpotential following a single AP or a train of APs (Maccaferri *et al.* 1993). Second, I_h may participate in the regulation of transmitter release, as proposed at the crayfish neuromuscular junction (Beaumont & Zucker, 2000) and at hippocampal mossy fibre terminals (Mellor *et al.* 2002). Finally, I_h is thought to be involved in rhythmogenesis. For example, I_h contributes to slow rhythmic activity in thalamocortical neurons (McCormick & Pape, 1990). By analogy, if I_h was expressed in fast-spiking GABAergic interneurons, it could have major influence on the AP phenotype, the properties of GABA release at interneuron output synapses, and the rhythmic properties of interneuron networks (Bartos *et al.* 2002; Vida *et al.* 2006). However, none of these hypotheses has been tested experimentally.

In this paper, we attempted to answer three questions. First, do fast-spiking BCs in the hippocampus express HCN channels? Second, if so, what is the subunit composition of these channels? Third, are HCN channels also expressed in axons or presynaptic terminals of fast-spiking GABAergic interneurons? We found that HCN channels are expressed in BCs of the dentate gyrus at both somatodendritic and axonal locations and that they shape both the input and the output properties of these cells.

Methods

Patch-clamp recording from dentate gyrus BCs in hippocampal slices

Transverse hippocampal slices (thickness, 300 μm) were cut from the brains of 17- to 21-day-old Wistar rats using a vibratome (Dosaka, Kyoto, Japan). Animals were killed by rapid decapitation without anaesthesias in accordence with national and institutional guidelines. Experiments were approved by the Animal Care Committe Freiburg according to §15 of the Tierschutzgesetz (registry T-04/10). Experiments were performed under visual control using infrared differential interference contrast videomicroscopy. BCs in the dentate gyrus were identified by the location of their soma in the granule cell layer near the hilar border and their fast-spiking AP phenotype (AP frequency for 800 ms, 1 nA pulses $>$ 50 Hz; Martina *et al.* 1998). Current- and voltage-clamp recordings were made with a Multiclamp 700A amplifier (Axon Instruments, Union City, CA, USA). Patch pipettes were pulled from thick-walled borosilicate glass tubing. When filled with internal solution, the resistance was 1.5–3 MΩ. Series resistance was 6–15 MΩ; it was compensated in current-clamp recordings, and carefully monitored but not compensated during voltage-clamp recordings. Signals were low-pass filtered at 2, 4 or 10 kHz (4-pole low-pass Bessel), and sampled at 5, 10 or 40 kHz. Pulse generation and data acquisition were performed using a 1401plus interface (CED, Cambridge, UK)/PC system with FPulse (home-made) running under Igor (version 5.01, Lake Oswego, OR, USA). In current-clamp experiments, the resting membrane potential was measured directly after obtaining access to the cell interior (-61.1 ± 0.3 mV; range, -65 to -54 mV; $n = 73$) and then set to -70 mV by injecting a constant negative holding current (≤ 150 pA). In voltage-clamp recordings, the holding potential was set to -50 mV. For antidromic AP propagation experiments, a stimulus electrode (glass pipette filled with Hepes-buffered Na^+-rich solution; resistance $\sim$1 MΩ) was placed in the granule cell layer at a distance of 200–1000 μm from the soma of the recorded BC. The stimulus intensity was 3–16 V and the stimulus duration was 0.2 ms. The location of the stimulation pipette tip was monitored carefully during the experiment, and the recording was terminated if a shift was observed. Effects of both ZD 7288 and Cs^+ were assessed between 10 and 30 min after onset of the application of the substance. The recording temperature was 21–24°C.

Recording of miniature IPSCs (mIPSCs) and GABA-activated currents in granule cells

mIPSCs in dentate gyrus granule cells were recorded in the whole-cell configuration in the presence of 1 μM TTX, 10 μM 6-cyano-7-nitroquinoxaline-2,3-dione

(CNQX) and 20 μM D-2-amino-5-phosphonopentanoic acid (D-AP5). The internal solution contained 140 mM KCl, and the holding potential was set to −70 mV. Currents activated by 10-ms pulses of 1 mM GABA were measured in outside-out and nucleated patches isolated from granule cells using fast-application techniques (Jonas, 1995). The exchange time (20–80%), measured with an open patch pipette during a change between 100% and 10% Hepes-buffered Na^+-rich external solution, was 200–300 μs for nucleated patch recordings (perfusion rate, 50–70 μl min^{-1}) and 50–150 μs for outside-out patches (perfusion rate, 200 μl min^{-1}). Pulses of GABA were applied every 5 or 8 s. Patches were held at −50 mV throughout the recordings.

Analysis

In current-clamp experiments, input resistance was determined from the voltage at the end of 800-ms hyperpolarizing current pulses. Apparent membrane time constants were measured by plotting voltage differences logarithmically in the range of 100% to 5% of the maximal amplitude, and fitting the final 20-ms epoch of each trace by linear regression. AP amplitude and half-duration were measured from the baseline preceding the current pulse. The maximal rate of rise was determined from the first derivative of the AP waveform. The fast afterhyperpolarization (AHP) amplitude was measured as the minimum voltage directly after the AP, the slow AHP was determined as the mean voltage after the fast AHP (∼18 ms after spike onset). AP frequency was determined as the inverse of the mean interspike interval. In voltage-clamp experiments, quantitative analysis of I_h was performed by digital subtraction of traces in the absence and presence of ZD 728 or Cs^+ (see Figs 3 and 4). Rise and decay of current traces were fitted by exponential functions. Conductance–voltage data were fitted with a Boltzmann function:

$$f = A\{1 + \exp[(V - V_{1/2})/k]\}^{-1} + (1 - A)$$

where A is the contribution of the voltage-dependent component, V is the membrane potential, $V_{1/2}$ is the midpoint potential and k is the slope factor. Activation and deactivation time constants were fitted with the function $\tau = 1/(\alpha + \beta)$, with $\alpha(V) = a\exp[V/k_1]$ and $\beta(V) = b\exp[-V/k_2]$, where a and b are rate constants at 0 mV and k_1 and k_2 are slope factors. Conductance was calculated as $G = I/(V - V_{rev})$, where I is current and V_{rev} is reversal potential. For display purposes, currents between 0 and 1 ms after voltage jumps were blanked. Fitting was made using the non-linear least-squares algorithms of Mathematica 4.1 (Wolfram Research, Champaign, IL, USA). P_{Na}/P_K was determined from V_{rev} according to the Goldman equation:

$$P_{Na}/P_K = -\left(c_{Ko} - c_{Ki}e^{V_{rev}F/RT}\right)/\left(c_{Nao} - c_{Nai}e^{V_{rev}RT}\right)$$

where c_{Ko}, c_{Ki} and c_{Nao}, c_{Nai} are outer and inner K^+ and Na^+ concentrations and F, R and T have standard thermodynamic meaning (Hille, 2001). Concentration–effect curves were fitted with the Hill equation:

$$f = I_{max}/(1 + IC_{50}/c)$$

where I_{max} is the blocked current, IC_{50} is half-maximal inhibitory concentration and c is concentration of ZD 7288 or Cs^+. mIPSCs in dentate gyrus granule cells were analysed as previously described, using a two-pass sliding template algorithm (Jonas *et al.* 1993; Clements & Bekkers, 1997). A template was shifted over a 100-s data section, sample point by sample point, and mIPSCs were detected based on predefined criteria for correlation coefficient ($r_{crit} > 0.5$) and peak amplitude ($a_{crit} > 10$ pA).

Solutions and chemicals

The physiological external solution contained (mM): NaCl 125 , $NaHCO_3$ 25, KCl 2.5, NaH_2PO_4 1.25, $CaCl_2$ 2, $MgCl_2$ 1 and glucose 25. The Hepes-buffered Na^+-rich external solution contained (mM): NaCl 135, KCl 5.4, $CaCl_2$ 1.8, $MgCl_2$ 1 and Hepes 5; pH adjusted to 7.2 with NaOH. The internal solution used in electrophysiological recordings contained (mM): KCl 140 or potassium gluconate 120 and KCl 20, EGTA 10, $MgCl_2$ 2, Na_2ATP 2 and Hepes 10; pH adjusted to 7.3 with KOH. The internal solution used for reverse transcription followed by quantitative polymerase chain reaction (RT-qPCR) experiments contained (mM): KCl 140, EGTA 5, $MgCl_2$ 3 and Hepes 5; pH adjusted to 7.3 with KOH. Chemicals were as follows: 4-ethylphenylamino-1,2-dimethyl-6-methylaminopyrimidinium chloride (ZD 7288, Tocris), 6-cyano-7-nitroquinoxaline-2,3-dione (CNQX, Tocris), D-2-amino-5-phosphonopentanoic acid (D-AP5, Tocris), bicuculline methiodide (BIC, Tocris), tetrodotoxin (TTX, Alomone), 4-aminopyridine (4-AP, Sigma) and γ-aminobutyric acid (GABA, Sigma).

Single-cell RT-qPCR

Single-cell expression analysis using RT-qPCR was performed as previously described (Monyer & Jonas, 1995; Franz *et al.* 2000; Lien *et al.* 2002; Liss, 2002). Patch-clamp capillaries were heated for 4 h at 220°C prior to use. After determining the AP phenotype in the whole-cell configuration, the cytoplasm of a recorded fast-spiking BC was harvested into the recording pipette. Experiments in which the gigaseal was disrupted or debris was attached to the outer surface of the

pipette were discarded. A 0.5-ml reaction tube was filled with 6 μl reverse transcription (RT) reaction buffer containing 1.4 × first strand buffer, 24 mM dithiothreitol (DTT), deoxynucleotidetriphosphates (dNTPs, 1.2 mM each), 1.7 × hexanucleotide mix (Hoffmann-La Roche, Basel, Switzerland) and 3 pmol Oligo(dT) primer. After expelling the contents of the patch pipette (~8 μl), the RT reaction was initiated by adding 100 U Superscript II (Invitrogen, Karlsruhe, Germany) and 20 U RNasin (Promega, Mannheim, Germany). After incubation for > 2 h at 37°C, cDNA was ethanol-precipitated in the presence of 1 μg glycogen (Ambion, Huntingdon, Cambridgeshire, UK), 250 ng poly(C) RNA (Amersham Biosciences, Freiburg, Germany) and 250 ng poly(dC) DNA (Amersham) with 0.1 vol 3 M Na acetate (pH 4.8) and 3.5 vol ethanol at −20°C overnight and followed by centrifugation (4°C, 20 000 *g*, 50 min). The supernatant was replaced by 100 μl 75% ethanol and then centrifuged again (4°C, 20 000 *g*, 40 min). After removal of the supernatant, the cDNA pellet was dried at 45°C, and resuspended in 8 μl sterile water (Sigma) and 27 μl of 2 × TaqMan MasterMix (Applied Biosystems, Darmstadt, Germany).

The cDNA solution of a single cell was split into two aliquots (16.5 μl), each used for the amplification of a single cDNA. Real-time qPCR was performed in a total volume of 25 μl with 880 nM primer (each) and 200 nM TaqMan probe in an ABI Prism 7000 sequence detection system (Applied Biosystems) using a default temperature cycle protocol (50°C for 2 min, 95°C for 10 min followed by 48 cycles with 95°C for 15 s and 60°C for 1 min). Primers and TaqMan probes were designed with PrimerExpress software (version 2.0; Applied Biosystems) and selected for maximal specificity and intron-overspanning amplicons. Sequences of primers and Taqman probes were as follows (F, forward; R, reverse; T, TaqMan probe; referring to published sequences in the GenBank of the National Center for Biotechnology Information, www.ncbi.nlm.nih.gov, HCN1, NM_053375; HCN2, NM_053684; HCN3, NM_053685; HCN4, NM_021658; neurofilament 3 (NF3), NM_017029; glial fibrillary acidic protein (GFAP), NM_017009):

HCN1–1641F	5′-GACGGCTCTTACTTTGGAGAAATATG-3′
	HCN1–1733R 5′-AAGGGAGTAAAGGCGACAGTATGT-3′
HCN1–1686T	5′-6Fam-CGCACTGCCAGTGTTCGAGCTGA-Tamra-3′
HCN2–1901F	5′-GCGTGCCTTTGAGACCGT-3′
HCN2–1979R	5′-CTGAACCTTGTGTAGCAAGATGGA-3′
HCN2–1929T	5′-6Fam-CGCCTGGACCGCATAGGCAAGAA-Tamra-3′
HCN3–1563F	5′-CAATGCAGTGCTTGAGGAGTTC-3′
HCN3–1689R	5′-GCCTGGACTCGGCTCAGA-3′
HCN3–1627T	5′-6Fam-TCTTTTTGCCGATGCGCCGAAG-Tamra-3′
HCN4–1404F	5′-CGCCTCATTCGGTACATTCA-3′
HCN4–1499R	5′-CATGCCAATGAGGTTCACGA-3′
HCN4–1458T	5′-6Fam-CTGGCCAGTGCCGTGGTACGC-Tamra-3′
NF3–1225F	5′-TCGCCGCATATAGGAAACTACTG-3′
NF3–1319R	5′-GGGCTGTCGGTGTGTGTACA-3′
NF3–1277T	5′-6Fam-TTCAGGAAGCATCACTGGGCCT-Tamra-3′
GFAP-784F	5′-GTGGTATCGGTCCAAGTTTGC-3′
GFAP-876R	5′-CGATAGTCATTAGCCTCGTGCTT-3′
GFAP-817T	5′-6Fam-CGTTGCTTCCCGCAACGCAGA-Tamra-3′.

The abundance of HCN1–4 transcripts was quantified on the basis of the interpolated cycle number in which fluorescence reached an arbitrary threshold of 0.2 fluorescence units (C_t value), using background fluorescence in cycles 7–29 as baseline. The relative abundance of HCN2 was calculated as $2^{-\Delta C_t}$, where $\Delta C_t = C_t(\text{HCN2}) - C_t(\text{HCN1})$, leading to normalization to the HCN1 expression level.

Several control experiments were performed to validate the results of RT-qPCR analysis. Amplification efficiency for HCN1–4 was assessed using cerebellar cDNA (mRNA extraction with DYNABeads, DYNAL, Oslo, Norway; cDNA synthesis as described for single-cell RT, 10-fold dilution); efficiency per cycle was 1.94 for HCN1, 1.97 for HCN2, 2.00 for HCN3 and 1.95 for HCN4. Possible differences in the amplification efficiencies for HCN1 and HCN2 were also tested using a plasmid containing both HCN1 and HCN2 fragments (2–200 plasmid copies per qPCR); C_t values under these conditions were almost identical ($C_t = 34.8 \pm 0.2$ and 34.9 ± 0.01 for 20 plasmid copies, $n = 3$). The molecular weight of the HCN1 and HCN2 amplicons from single-cell RT-qPCR was examined on ethidium bromide-stained agarose-TAE gels; sizes were in close agreement with the expected length. In some cases, amplicons were verified by cloning into a pBluescript SK$^-$ vector (Stratagene, La Jolla, CA, USA) followed by sequencing. To exclude the possibility of contaminations, sterile water controls were run in parallel to every qPCR, and the reverse transcriptase was omitted in a subset of cells. No amplification signal was detected after 48 qPCR cycles under these conditions.

Statistical analysis

Data are reported as mean ± S.E.M.; error bars in the Figures also represent S.E.M. and are shown only if they exceeded the size of the symbol. Statistical significance was assessed using a two-sided Wilcoxon signed rank test for paired samples at a given significance level (P).

Results

ZD 7288 affects passive, but not active membrane properties of fast-spiking BCs

We examined the contribution of I_h to the resting membrane properties of fast-spiking BCs in the dentate gyrus under current-clamp conditions (Fig. 1). To minimize cell-to-cell variability, the initial resting potential of recorded neurons was set to −70 mV by

injection of hyperpolarizing current. Although a sag during hyperpolarizing current pulses was not apparent under these conditions (Fig. 1*A* and *B*; Maccaferri & McBain, 1996; Lupica *et al.* 2001), bath application of the I_h channel blocker ZD 7288 at a concentration of 30 μM led to a hyperpolarization of the membrane potential by 5.7 ± 1.5 mV ($P < 0.05$; $n = 6$ BCs). Correlated with the hyperpolarization, the somatic input resistance, measured from the voltage deflection at the end of a hyperpolarizing 100-pA, 800-ms current pulse, increased from 64.3 ± 8.6 to 106.6 ± 15.0 MΩ ($P < 0.05$; Fig. 1*C*–*F*). Furthermore, the apparent membrane time constant measured by logarithmic fitting of the responses to hyperpolarizing current pulses increased from 12.5 ± 0.8 to 71.6 ± 8.0 ms ($P < 0.05$; Fig. 1*B* and *G*). As reported previously (Harris & Constanti, 1995; Beaumont & Zucker, 2000; Chevaleyre & Castillo, 2002), the effects of ZD 7288 were largely irreversible after washout (Fig. 1*C* and *D*). Thus, the I_h channel blocker ZD 7288 hyperpolarized fast-spiking BCs, increased their input resistance and prolonged their apparent membrane time constant, consistent with a contribution of I_h to resting membrane characteristics.

We next tested whether the I_h channel blocker ZD 7288 affected active membrane properties, using the amplitude and shape of single APs and the maximal AP frequency during trains of spikes as parameters (Fig. 2). Without compensation for the ZD 7288-induced hyperpolarization

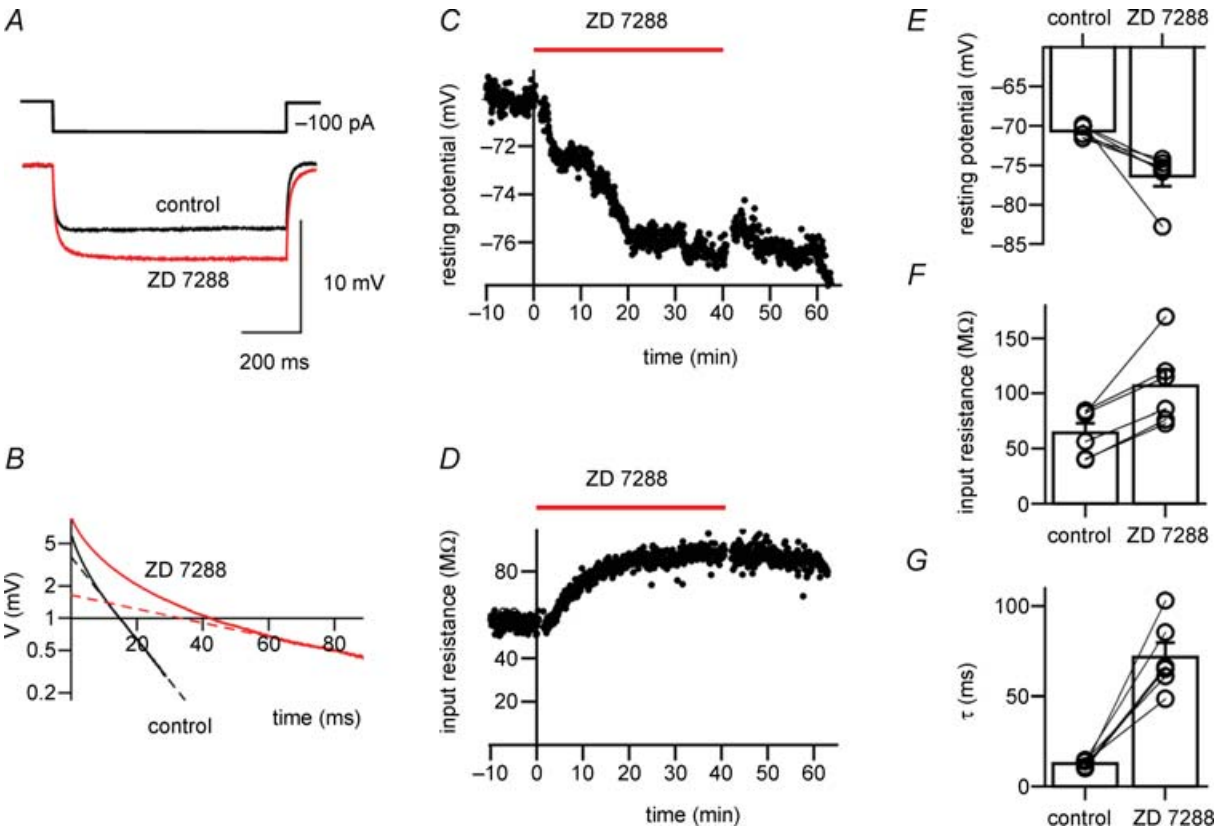

Figure 1. ZD 7288 induces hyperpolarization, increases input resistance and prolongs apparent membrane time constant of fast-spiking BCs

A, voltage traces recorded during hyperpolarizing current pulses (−100 pA). Black trace, control; red trace, 30 μM ZD 7288. Average of 50 and 20 sweeps, respectively. The hyperpolarization of the resting membrane potential occurring during application of ZD 7288 was subtracted from the traces. *B*, corresponding semilogarithmic plot of voltage *versus* time during −100 pA current pulses. Apparent membrane time constants were measured by plotting voltage differences logarithmically in the range 100% to 5% of the maximal amplitude, and fitting the final 20-ms epoch of each trace by linear regression (dashed lines). Time constants τ were 11.2 ms in control and 66.4 ms in the presence of ZD 7288. *C*, graph of resting potential *versus* time during application of 30 μM ZD 7288. *D*, corresponding graph of input resistance *versus* time, measured with hyperpolarizing current pulses. Horizontal bars in *C* and *D* represent the duration of the application of ZD 7288. Data in *A*–*D* are from the same cell. *E*–*G*, summary bar graphs of the effects of 30 μM ZD 7288 on resting membrane potential (*E*), input resistance (*F*) and apparent membrane time constant (τ) determined by logarithmic fitting (*G*) in six BCs. Bars represent mean values, circles connected by lines indicate data from the same experiment. In all experiments, 10 μM CNQX, 20 μM D-AP5, and 20 μM BIC were added to the bath solution to block synaptic events.

(see Fig. 1*C*), 30 μM ZD 7288 led to a significant decrease in the fast and slow AHP of single APs elicited by 0.5-ms current pulses (from -3.7 ± 0.5 to -0.9 ± 0.4 mV and from -1.4 ± 0.2 to 1.9 ± 0.5 mV; $P < 0.005$ in both cases; $n = 10$ BCs), whereas the maximal rate of rise, the peak amplitude and the half-duration were unchanged ($P > 0.1$). In contrast, when the somatic membrane potential was held at -70 mV by continuous adjustment of the holding current during application of the blocker (Fig. 2), ZD 7288 had no significant effects on the measured parameters (Fig. 2*C*–*G*; $P > 0.1$). As the maximal rate of rise of the AP is dependent on the Na^+ current, whereas the half-duration is correlated with the K^+ current, these results indicate that voltage-gated Na^+ and K^+ channels are unaffected by ZD 7288. Furthermore, ZD 7288 had no effects on the maximal AP frequency in trains of spikes evoked by long current pulses (800 pA, 800 ms) under these conditions (Fig. 2*B* and *H*). Thus, although previous studies suggested that ZD 7288 may alter conductances other than I_h with high concentrations and long application times (Chen, 2004; see also Chevaleyre & Castillo, 2002), 30 μM ZD 7288 had no detectable effects on the active membrane properties of fast-spiking interneurons.

Pharmacological properties, ion selectivity and gating of I_h expressed in BCs

We next examined I_h expressed in BCs under voltage-clamp conditions (Fig. 3). Test pulses from a holding potential of -50 mV to a potential of -120 mV activated an inward current with time-dependent onset (Fig. 3*A*). ZD 7288 at a concentration of 1–100 μM blocked this current in a concentration-dependent manner. Plotting the amplitude of the ZD 7288-sensitive current against ZD 7288 concentration revealed a

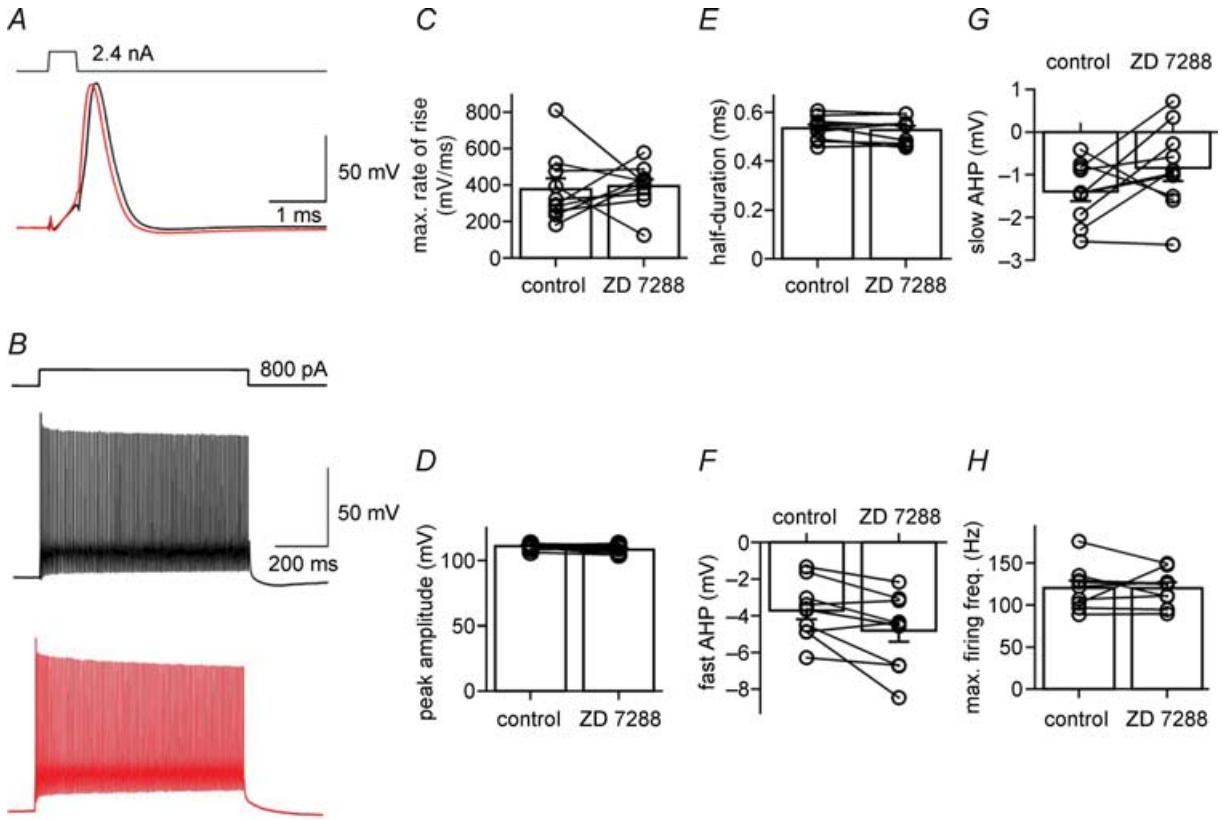

Figure 2. ZD 7288 affects passive, but not active membrane properties of fast-spiking BCs
A, traces of APs evoked by 2.4 nA, 0.5-ms current pulses. Black trace, control; red trace, 30 μM ZD 7288. The cell was held at -70 mV by holding current adjustment throughout the experiment. *B*, traces of APs evoked by 800-pA, 800-ms current pulses. Black trace, control; red trace, 30 μM ZD 7288. *C*–*G*, summary graphs of the effects of ZD 7288 on maximal rate of rise (*C*), AP peak amplitude (*D*), AP duration at half-maximal amplitude (*E*), fast afterhyperpolarization (AHP) (*F*) and slow AHP (*G*). All parameters were measured for single APs evoked by brief current pulses. *H*, summary graph of the effects of ZD 7288 on maximal AP frequency. Frequency was determined for trains of APs evoked by 800-pA, 800-ms pulses. Bars represent mean values, circles indicate data from individual experiments. Data from 10 BCs. In all experiments, 10 μM CNQX, 20 μM D-AP5 and 20 μM BIC were added to the bath solution.

half-maximal inhibitory concentration of 1.4 μM and a Hill coefficient of 1.3 ($n = 9$ BCs; Fig. 3*B*). Thus, ZD 7288 blocked hyperpolarization-activated currents in fast-spiking BCs with micromolar affinity. Both recombinant and native I_h channels are also blocked by external Cs^+ (Santoro *et al.* 1998; Chevaleyre & Castillo, 2002). We therefore tested whether external Cs^+ was able to mimic the effects of ZD 7288 in fast-spiking BCs (Fig. 3*C*). As with ZD 7288, 30–3000 μM Cs^+ blocked the hyperpolarization-activated inward current in a concentration-dependent manner. The half-maximal inhibitory concentration was 37 μM, and the Hill coefficient was 1.1 ($n = 5$ BCs; Fig. 3*D*). These results show that fast-spiking BCs express a hyperpolarization-activated conductance with pharmacological properties characteristic of I_h. Subtraction of currents under control conditions and in the presence of saturating concentrations of either ZD 7288 or Cs^+, revealed both an instantaneous and a time-dependent component of I_h during test pulses (Fig. 3*E*). Both components were blocked with comparable concentration dependence and time course

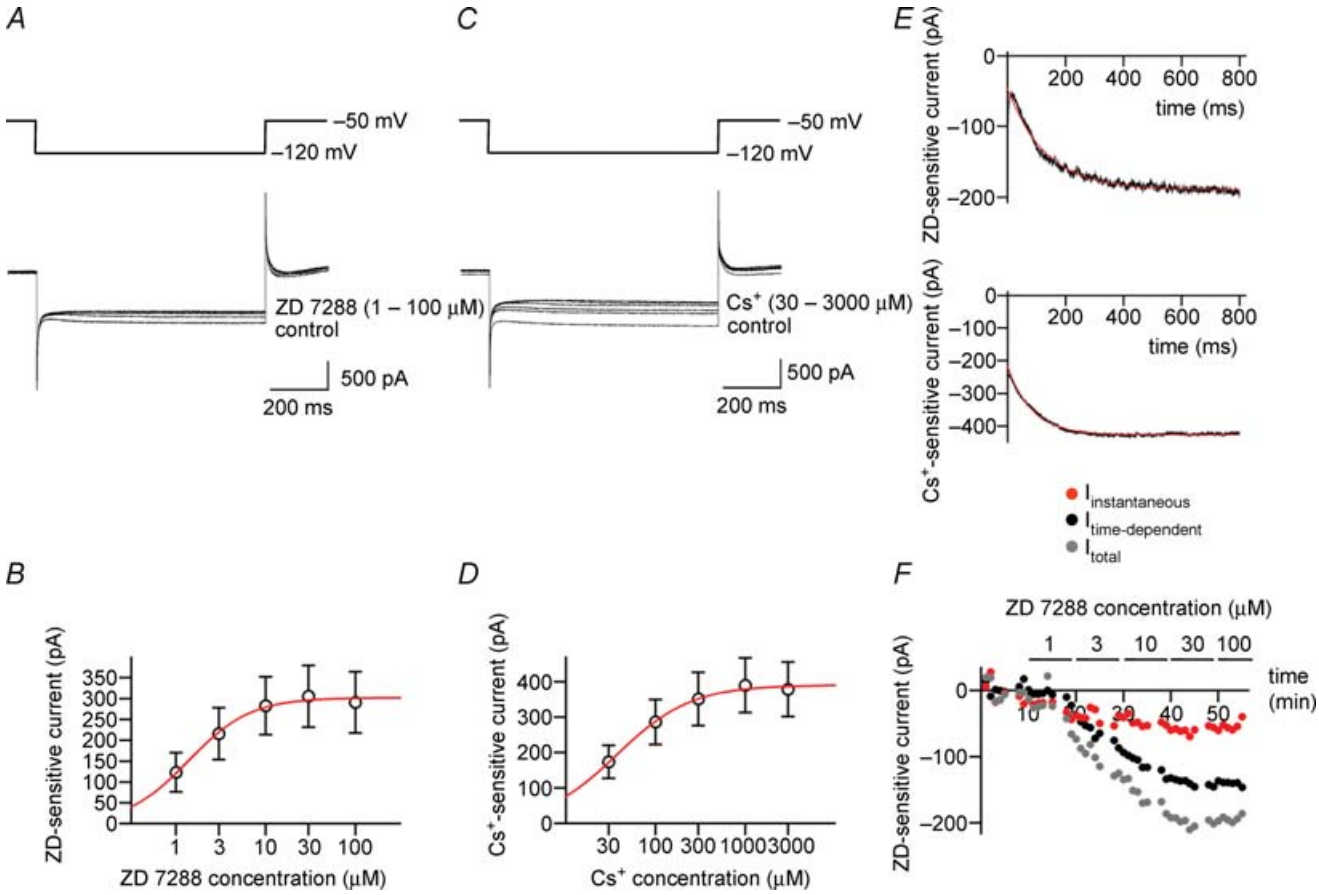

Figure 3. Both external ZD 7288 and Cs^+ block hyperpolarization-activated currents in BCs in a concentration-dependent manner

A, traces of currents activated by hyperpolarizing pulses from a holding potential of −50 mV to a test pulse potential of −120 mV in the presence of different concentrations of ZD 7288 in the bath solution. *B*, amplitude of the ZD 7288-sensitive current, plotted against ZD 7288 concentration. Data points were fitted with a Hill equation, yielding an IC_{50} of 1.4 μM and a Hill coefficient of 1.3. Data from nine BCs. *C*, traces of currents activated by hyperpolarizing pulses from −50 to −120 mV in the presence of different concentrations of Cs^+ in the bath solution. *D*, amplitude of the Cs^+-sensitive current, plotted against Cs^+ concentration. IC_{50}, 37.4 μM; Hill coefficient, 1.1. Data from five BCs. *E*, onset time course of ZD 7288-sensitive current (upper trace) and Cs^+-sensitive current (lower trace) obtained by digital subtraction of currents in the absence and in the presence of 100 μM ZD 7288 and 3 mM Cs^+, respectively. Note instantaneous and time-dependent component. Red curves, fitted exponential functions. *F*, graph of amplitude of total I_h (grey circles), instantaneous component (red circles) and time-dependent component (black circles) during application of different concentrations of ZD 7288 (horizontal bars). Data in *A*, *E* and *F* are from the same BC. ZD 7288- and Cs^+-sensitive currents were isolated by digital subtraction of traces before and after application of different concentrations of ZD 7288 and Cs^+, respectively. In all experiments, 1 μM TTX, 3 mM 4-AP, 10 μM CNQX, 20 μM D-AP5 and 20 μM BIC were added to the bath solution.

(Fig. 3*F*). For I_h isolated by subtracting currents ~20 min after application of 30 μM ZD 7288 from those under control conditions, the relative contribution of the instantaneous component was $34 \pm 8\%$ ($n = 8$ BCs), suggesting that a fraction of I_h channels is open at the holding potential of −50 mV (Macri & Accili, 2004; Rodrigues & Oertel, 2006).

We next determined the ion selectivity and the gating properties of I_h expressed in fast-spiking BCs (Fig. 4). To examine the ion selectivity, a prepulse to −120 mV was applied from a holding potential of −50 mV to maximally activate the channels, followed by a test pulse to potentials between −110 and −60 mV to determine the current reversal potential (Fig. 4*A*). I_h was isolated pharmacologically by subtracting currents in the presence of 30 μM ZD 7288 from those under control conditions. The current at the beginning of the test pulse was plotted against test-pulse voltage, and analysed by linear regression. Under the ionic conditions used, the extrapolated reversal potential was −27.4 mV ($n = 8$ BCs; Fig. 4*B*), corresponding to P_{Na}/P_K of 0.36. Thus, I_h channels expressed in fast-spiking BCs are non-selective cation channels with moderate selectivity for K^+ over Na^+.

To determine the voltage dependence of activation of I_h, test pulses to potentials between −60 and −120 mV were applied from a holding potential of −50 mV (Fig. 4*C*). The activation curve was obtained from the total current at the end of the test pulse, which was converted into conductance using the current reversal potential determined previously in the same cell. Fitting the data with a Boltzmann function gave a midpoint potential of −83.9 mV and a slope factor of 13.1 mV, with a small voltage-independent component of 0.08 ($n = 8$ BCs; see Methods; Fig. 4*D*). Activation and deactivation time courses were further analysed by fitting the rise and decay phase of the current at different test-pulse amplitude with exponential functions (Fig. 4*E*). The activation time constant measured at −120 mV was 190.4 ± 23.1 ms, while the deactivation time constant at −50 mV was

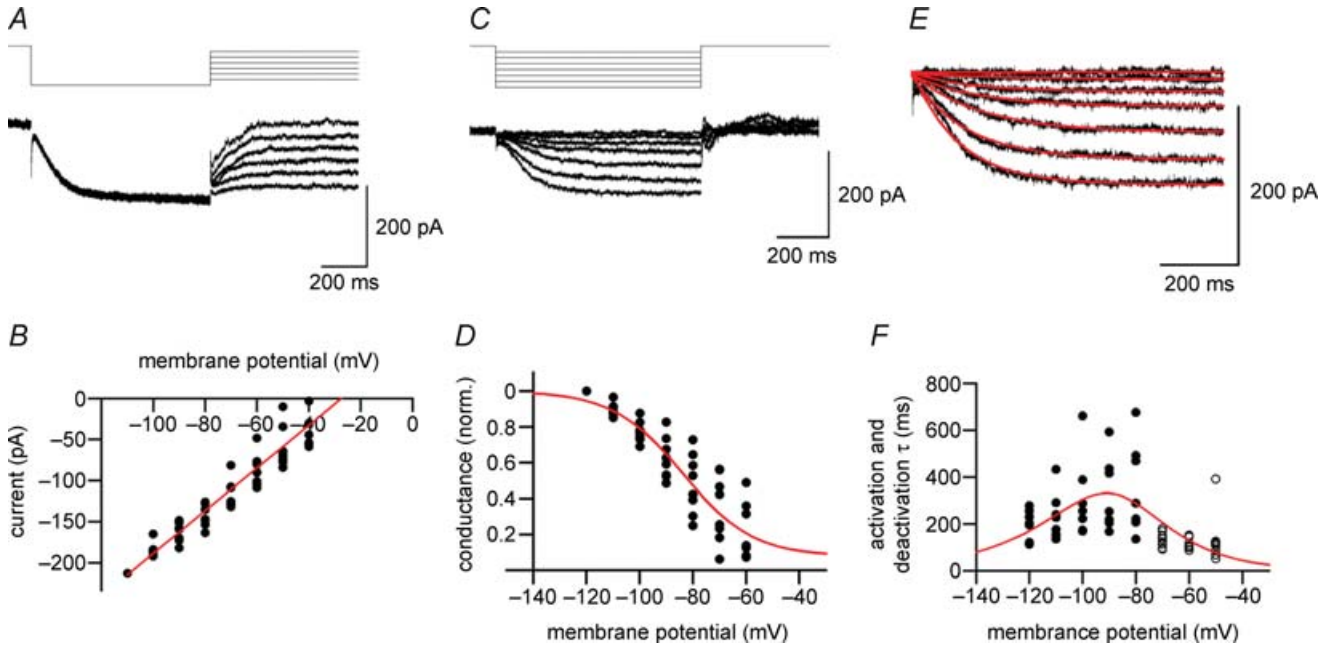

Figure 4. Ion selectivity and gating properties of hyperpolarization-activated currents in BCs
A, traces of ZD 7288-sensitive currents activated by a hyperpolarizing prepulse to −120 mV, followed by a test pulse to potentials between −110 and −60 mV. Holding potential, −50 mV. *B*, instantaneous current–voltage relation obtained by plotting the current at the beginning of the test pulse against test pulse potential. Currents were normalized to the value at −110 mV, and remultiplied by the respective mean. Red line obtained by linear regression. Extrapolated reversal potential, −27.4 mV. *C*, traces of ZD 7288-sensitive currents activated by hyperpolarizing test pulses between −120 and −60 mV. Holding potential, −50 mV. *D*, I_h channel activation curve. I_h was measured as the total current at the end of the test pulses, converted into conductance, and normalized to the value at −120 mV. Red curve, fitted Boltzmann function (midpoint potential, −83.9 mV; slope, 13.1 mV; voltage-independent component, 0.08). *E*, traces of I_h at potentials between −120 and −60 mV (protocol as in *C*). Red curves, fitted exponentials. *F*, time constants of activation (●) and deactivation (○). Time constants were determined by fitting traces with single exponential functions. Red curve, fitted τ function (see Methods). Data in *B*, *D* and *F* are from eight BCs. ZD 7288-sensitive currents were isolated by digital subtraction of traces before and after application of 30 μM ZD 7288. In all experiments, 1 μM TTX, 3 mM 4-AP, 10 μM CNQX, 20 μM D-AP5 and 20 μM BIC were added to the bath solution.

133.8 ± 37.9 ms. Plotting activation and deactivation time constants against voltage revealed a bell-shaped relationship with a maximal value at approximately −90 mV ($n = 8$ BCs; Fig. 4*F*), comparable to the midpoint potential of the activation curve.

I_h channels expressed in fast-spiking BCs are likely assembled from HCN1 and HCN2 subunits

To examine the putative subunit composition of the native I_h channels, we analysed the expression of HCN1–4 subunit mRNA in fast-spiking BCs by single-cell RT-qPCR (see Methods; Fig. 5). The harvested cytoplasm from each single cell was reverse transcribed, and the resulting cDNA was split into two aliquots. The first aliquot was amplified with primers for one of the HCN subunits, whereas the second aliquot was amplified with primers for another HCN subunit, NF3 or GFAP. Single-cell RT-qPCR analysis revealed that fast-spiking BCs expressed HCN1 and HCN2 (Fig. 5*A*), whereas HCN3 and HCN4 were not detectable (Fig. 5*B* and *C*). In 5 of 5 BCs tested with primers for HCN1 and HCN2, both HCN subunits were coexpressed in the same cell, suggesting the formation of heteromeric channels (Chen *et al.* 2001). The HCN2/HCN1 cDNA ratio, quantified using the difference in C_t values in the qPCR (Fig. 5*A*, inset), was 0.61 ± 0.14 ($n = 5$ BCs; Fig. 5*D*). Cells tested were positive for NF3, but negative for GFAP, as expected for selective harvesting from neurons ($n = 3$ BCs). To summarize, single-cell RT-qPCR revealed that fast-spiking BCs coexpress HCN1 and HCN2 transcripts with comparable relative abundance, whereas HCN3 and HCN4 transcripts were not detectable.

Evidence for the presence of I_h in axons and presynaptic terminals of fast-spiking BCs

Previous studies suggested that I_h is present in both peripheral and central axons (Baker *et al.* 1987; Soleng *et al.* 2003). We therefore probed the possible axonal localization of I_h in fast-spiking BCs (Fig. 6). The BC axon was stimulated extracellularly, and antidromic APs were recorded at the soma under current-clamp conditions

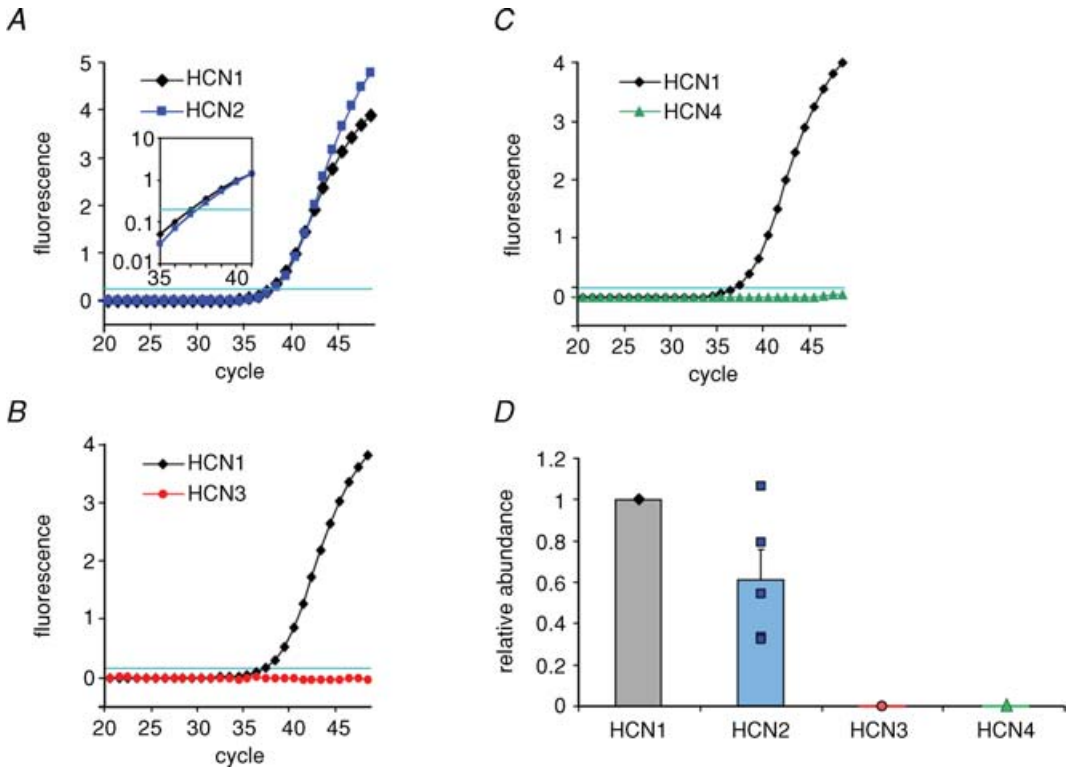

Figure 5. Single-cell RT-qPCR reveals that BCs coexpress HCN1 and HCN2 subunits
A–C, detection of HCN subunits by RT-qPCR analysis. The mRNA of the material harvested from a single cell was reverse-transcribed, and the resulting cDNA was split into two aliquots to examine the coexpression of two HCN subunits in a given cell. Note that BCs coexpressed HCN1 and HCN2, but lacked detectable expression of HCN3 and HCN4. Inset in *A* is logarithmic plot of fluorescence between cycle 35 and 41, illustrating a difference in C_t value (i.e. cycle number in which fluorescence reaches an arbitrary threshold of 0.2; horizontal lines in *A–C*). *D*, relative abundance of HCN1–4 cDNA in single BCs. For each subunit, relative abundance was quantified as $2^{-\Delta C_t}$, where $\Delta C_t = C_t$ (HCN2) − C_t(HCN1). Data from 11 BCs.

while the resting potential was held at −70 mV by continuous adjustment of the holding current (Fig. 6*A*). Under control conditions, suprathreshold stimuli evoked APs with 100% reliability (Fig. 6*B*). With the same stimulus intensity, bath application of 30 μM ZD 7288 reduced the reliability of AP initiation and finally abolished antidromic spikes (Fig. 6*C*). To distinguish between stimulation and conduction failures, the stimulus intensity was increased. AP initiation was restored under these conditions, arguing for stimulation rather than conduction failures (Fig. 6*D*). To quantify this observation, the probability of evoking an AP was plotted against stimulus intensity (Fig. 6*E*). ZD 7288 (30 μM) increased the current threshold (defined as the current leading to 50% successes) to 155 ± 8% of the control value ($P < 0.05$; $n = 6$ BCs; Fig. 6*F*). As a block of I_h would be expected to hyperpolarize the axon, which in turn would increase the threshold of AP initiation, these results suggest axonal localization of I_h in fast-spiking BCs.

In both the calyx of Held and in cerebellar Pinceau terminals, I_h is expressed presynaptically (Southan *et al.* 2000; Cuttle *et al.* 2001). To examine whether I_h is also present in presynaptic terminals of BCs, we recorded mIPSCs in granule cells, the main target cells of BCs in the dentate gyrus (Fig. 7). mIPSCs were recorded in the presence of 1 μM TTX, 10 μM CNQX and 20 μM D-AP5, and were detected using a sliding template algorithm (Fig. 7*A* and *B*). Under control conditions, the mean frequency of mIPSCs was 1.82 ± 0.35 Hz, and the mean peak amplitude was 58.7 ± 1.5 pA. After application of 30 μM ZD 7288, the frequency was reduced to 69.6 ± 4.0% of the control value (1.12 ± 0.16 Hz; $P < 0.001$; $n = 15$ granule cells), whereas the amplitude was not significantly affected (57.2 ± 1.8 pA; $P > 0.1$; Fig. 7*C*–*F*). The fast rise time of the mIPSCs (20%–80% rise time: control, 0.74 ± 0.07 ms; ZD 7288, 0.70 ± 0.07 ms; $P > 0.8$) suggests that these events were mainly generated in

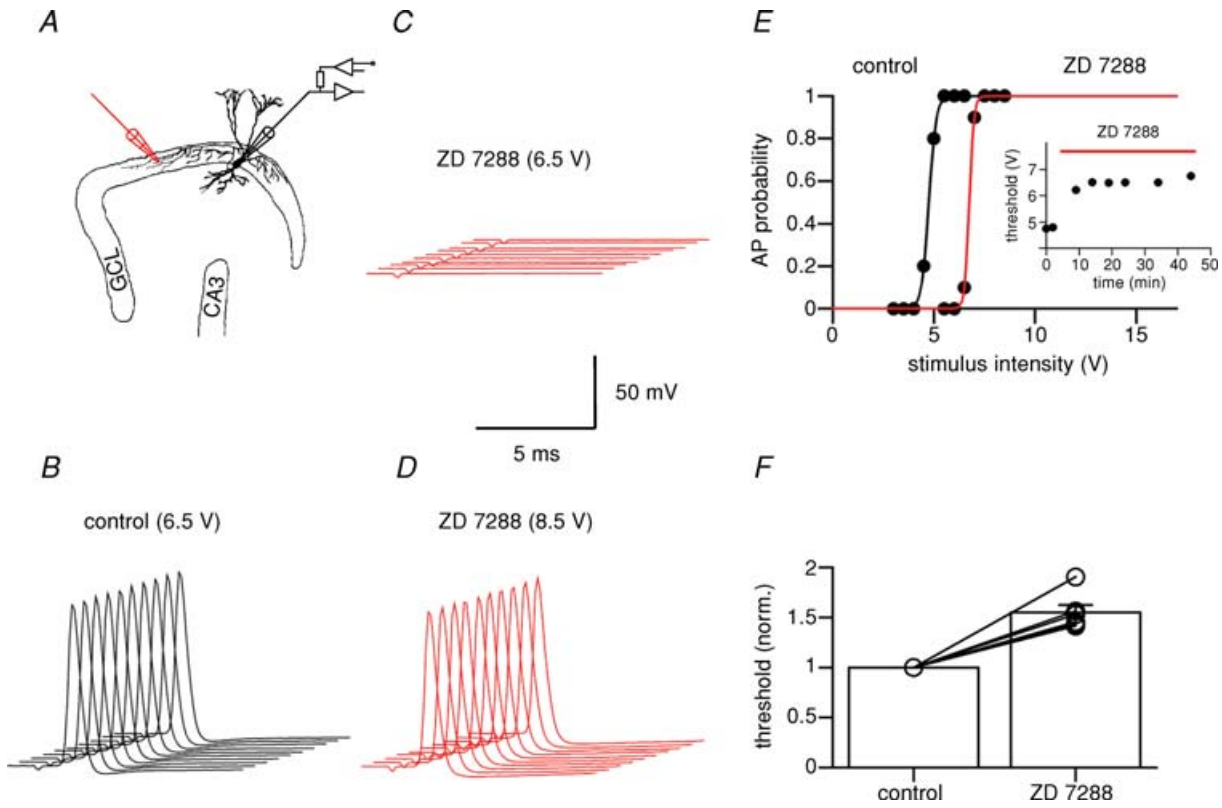

Figure 6. I_h channel block increases the threshold of AP initiation in BC axons
A, schematic illustration of stimulation and recording configuration. A stimulus electrode (monopolar glass pipette) was placed in the granule cell layer (GCL) at a distance of 200–1000 μm from the recorded BC. *B*–*D*, 10 consecutive APs in control conditions (*B*, stimulus intensity 6.5 V), in the presence of 30 μM ZD 7288 at the same stimulus intensity (*C*), and in the presence of ZD 7288 after increase in stimulation intensity (*D*, 8.5 V). The somatic resting potential in the recorded BC was maintained at −70 mV by continuous adjustment of the holding current. Traces were right-upwardly shifted against each other for clarity. *E*, probability of AP initiation plotted against stimulus intensity in control conditions (black) and after application of 30 μM ZD 7288 (red). Note that ZD 7288 increased the threshold for AP initiation. Curves show Boltzmann functions fitted to the data points. Inset shows AP initiation threshold plotted against time during ZD 7288 application for the same cell. *F*, summary of the effects of ZD 7288 on AP threshold. Data from six BCs. In all experiments, 10 μM CNQX, 20 μM D-AP5 and 20 μM BIC were added to the bath solution to block synaptic events.

the perisomatic region of granule cells (Soltesz *et al.* 1995).

A previous study suggested that ZD 7288 blocks AMPA-type glutamate receptors (Chen, 2004). To exclude the possibility that direct effects on $GABA_A$ receptors interfered with an accurate estimate of mIPSC frequency and amplitude, we tested the effects of 30 μM ZD 7288 on currents activated by fast application of GABA to patches isolated from granule cells (Fig. 7*G*). ZD 7288 (30 μM) had no effects on amplitude and kinetics of the GABA-activated currents; in the presence of ZD 7288, the peak amplitude was $100.9 \pm 5.3\%$ of the control value ($P > 0.8$; $n = 5$ granule cells; Fig. 7*H*). Thus, our results are consistent with a presynaptic effect of ZD 7288, presumably at BC terminals.

Discussion

Our results shed light on the role of I_h in shaping the integrative properties and the synaptic output of fast-spiking BCs in the hippocampus. First, we found that fast-spiking BCs expressed HCN channels, and that these channels contributed to resting potential, input resistance and apparent membrane time constant. Second, quantitative single-cell RT-qPCR suggested that these channels were heteromers composed of HCN1 and HCN2 subunits. Finally, antidromic stimulation and mIPSC experiments suggested that HCN channels were not only expressed in the somatodendritic domain of GABAergic interneurons, but were also present in axons and presynaptic terminals, where they may be involved in the regulation of GABA release.

Functional properties and subunit composition of I_h channels in BCs

Previous studies suggested that ZD 7288, in addition to blocking I_h channels, affects AMPA-type glutamate receptors (Chen, 2004). However, several lines of evidence

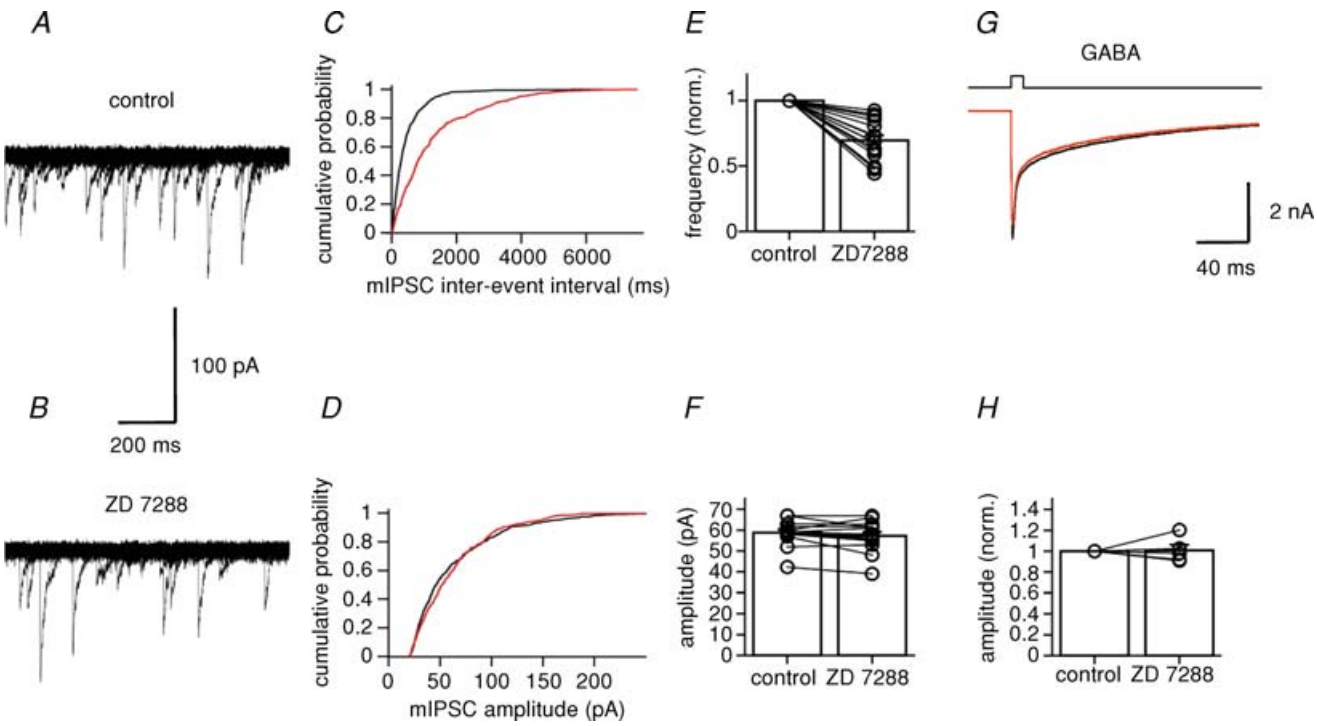

Figure 7. I_h channel block reduces the frequency of miniature IPSCs in granule cells
A, 20 consecutive traces of spontaneous mIPSCs recorded in a granule cell at −70 mV under control conditions. *B*, similar traces after application of 30 μM ZD 7288. For display purposes, recorded traces were digitally filtered at 1 kHz. *C*, cumulative histograms of mIPSC interevent interval. *D*, cumulative histograms of mIPSC peak amplitude. Black curves, control; red curves, 30 μM ZD 7288. Data shown in *A–D* were obtained from the same cell. *E* and *F*, summary bar graphs showing the effects of ZD 7288 on mIPSC frequency (normalized to control values, *E*) and amplitude (*F*). Left bar, control; right bar, 30 μM ZD 7288. Data from 15 granule cells. Bars represent mean values, circles represent data from individual experiments. In all experiments, 1 μM TTX, 10 μM CNQX and 20 μM D-AP5 were added to the bath solution. *G*, currents activated by fast application of 1 mM GABA (10-ms pulse) to a nucleated patch isolated from a granule cell. Holding potential, −50 mV. Black trace, control (pulse from Na^+-rich solution to Na^+-rich solution + 1 mM GABA); red trace, 30 μM ZD 7288 (pulse from Na^+-rich solution + 30 μM ZD 7288 to Na^+-rich solution + 30 μM ZD 7288 + 1 mM GABA). Each trace is the average of 20 single sweeps. *H*, summary bar graph showing the lack of effects of ZD 7288 on GABA-activated currents ($n = 5$ patches).

suggest that the block of I_h in fast-spiking BCs is relatively specific. First, I_h was blocked by both ZD 7288 and external Cs^+. Second, ZD 7288 had no effects on the rate of rise and the duration of the AP in fast-spiking interneurons, suggesting that it does not affect voltage-gated Na^+ and K^+ channels. Finally, ZD 7288 did not change the amplitude of currents activated by fast application of GABA, showing that it does not affect $GABA_A$ receptors. Therefore, the use of ZD 7288 to isolate pharmacologically I_h in voltage-clamp experiments appears to be justified.

How do the functional properties of I_h channels expressed in fast-spiking BCs compare to those expressed in other types of central neurons? I_h channels in BCs are non-selective cation channels with a slight preference for K^+ over Na^+ ions. P_{Na}/P_K is 0.36, similar to I_h reported in other cell types (e.g. 0.36 in photoreceptors; Wollmuth & Hille, 1992; see also DiFrancesco, 1981). Furthermore, the midpoint potential of the activation curve of the time-dependent component of I_h is −83.9 mV. This is also comparable to values found in other cell types (−90 to −83 mV; Franz *et al.* 2000). Thus, I_h expressed in fast-spiking BCs shows an ion selectivity and a voltage range of activation similar to other types of neurons.

The activation time constant of I_h channels expressed in fast-spiking BCs is 190 ms at −120 mV and 21–24°C. This is slower than I_h in hippocampal CA1 pyramidal neurons (64 ms) and neocortical layer 5 pyramidal neurons (84 ms), but faster than in substantia nigra dopaminergic neurons (482 ms) and thalamocortical neurons (602 ms; 22–24°C; Franz *et al.* 2000). When recombinantly expressed in host cells, HCN1 shows the fastest gating, whereas HCN4 shows the slowest gating (time constants, HCN1 < HCN2 ∼ HCN3 < HCN4; Santoro *et al.* 2000; Chen *et al.* 2001). Thus, the intermediate gating kinetics of I_h in BCs is consistent with the idea that the native channel is an HCN1/HCN2 heteromer, as suggested by RT-qPCR analysis.

Both ZD 7288- and Cs^+-sensitive currents evoked by hyperpolarizing test pulses from a holding potential of −50 mV showed an instantaneous and a time-dependent current component (Fig. 3*E*). In ZD 7288-sensitive currents, the relative contribution of the instantaneous component was 34%. As the instantaneous component was evident in both ZD 7288- and Cs^+-sensitive currents, it seems unlikely that it is mediated by a channel other than I_h. Despite considerable variability across cells, our results suggest two contributions to this instantaneous component. First, the activation curve given by the fitted Boltzmann function is relatively shallow (slope factor, 13.1 mV), implying that I_h is not completely deactivated at −50 mV. Second, the activation curve shows a voltage-independent component (Fig. 4*D*). These results are consistent with the hypothesis that I_h channels expressed in fast-spiking BCs are heterogeneous, with one subpopulation activating and deactivating in a time- and voltage-dependent manner and another subpopulation constitutively open. Instantaneous components in the ZD 7288-sensitive current have been recently reported for both recombinant (Macri & Accili, 2004; Proenza & Yellen, 2006) and native HCN channels (Day *et al.* 2005; Rodrigues & Oertel, 2006). However, in recombinant channels the instantaneous component appears to be sensitive to ZD 7288, but not Cs^+ (Macri & Accili, 2004).

HCN channels shape integrative properties of fast-spiking interneurons

Our results indicate that I_h channels contribute to the low input resistance and the fast apparent membrane time constant of dentate gyrus BCs. As the decay of EPSPs is shaped by the membrane time constant, HCN channels will limit the duration of EPSPs, and thereby sharpen the temporal window for coincidence detection of synaptic inputs (Geiger *et al.* 1997; Jonas *et al.* 2004; Yamada *et al.* 2005). Thus, the expression of I_h will contribute to the repertoire of fast signalling mechanisms in fast-spiking BCs (Jonas *et al.* 2004).

Our results further suggest that I_h channels shape the input–output relation of fast-spiking BCs. As I_h channels are non-selective cation channels, they will shift the membrane potential away from the resting potential into the depolarizing direction. However, their activation by hyperpolarization also implements a negative feedback loop. If depolarization is too large, I_h channels will deactivate, and the membrane potential will return to the original resting value. Thus, the interneurons are clamped at a subthreshold potential, setting them into a ready-to-fire mode from which APs can be triggered readily. In this scenario, despite the low input resistance of BCs, activation of a small number of excitatory synaptic inputs is sufficient to trigger an AP (Geiger *et al.* 1997).

The presence of a sag during hyperpolarizing current injection is thought to be the hallmark of neurons expressing I_h (Pape, 1996; Robinson & Siegelbaum, 2003). However, although I_h channels are expressed in BCs, a pronounced sag under current-clamp conditions is not evident. Thus, our results show that the correlation between sag and I_h expression is not absolute. Two factors may explain this apparent discrepancy. First, the activation kinetics of the time-dependent component of I_h in BCs temporally overlaps with a slow component of the membrane time constant uncovered by ZD 7288 application (Fig. 1*A* and *B*). Second, the relatively shallow voltage dependence of the activation curve (Fig. 4*D*) implies relatively small changes in open probability of I_h during hyperpolarizing current pulses.

HCN channels are present in axons and presynaptic terminals of fast-spiking interneurons

In experiments in which APs were evoked by extracellular axonal stimulation, ZD 7288 increased the proportion of AP failures. Antidromic spikes were restored by increasing stimulus intensity, suggesting failures of initiation rather than failures of conduction. The simplest interpretation of these findings is that block of I_h channels hyperpolarizes the axon, and thereby increases the threshold for AP initiation by brief extracellular stimuli. The physiological significance of the presence of HCN channels in axons is not known. One possibility is that I_h increases the reliability of AP propagation in fine axonal branches (reviewed by Debanne, 2004). This may be relevant for the propagation of APs in BC axons, which arborize very extensively (Freund & Buzsáki, 1996). In Schaffer collateral axons, it was proposed that I_h compensates for the hyperpolarization induced by the activity of the electrogenic Na^+–K^+-ATPase (Soleng *et al.* 2003). Considering the high AP frequency and metabolic rate of BCs, I_h may have a similar function in these neurons.

Our results further suggest that I_h is present in inhibitory presynaptic terminals. ZD 7288 reduced the frequency of mIPSCs in dentate gyrus granule cells. Although these neurons receive inhibitory input from several types of interneurons (Freund & Buzsáki, 1996), previous studies suggested that mIPSCs in granule cells mainly originate from synapses located close to the soma (Soltesz *et al.* 1995). Thus, it is likely that the effects of ZD 7288 on mIPSCs in granule cells are generated mainly via block of I_h channels, located either in BC terminals or electrotonically close to these terminals. The present data differ from results in both the hippocampal CA1 region and the cerebellum, where ZD 7288 changes the frequency of spontaneous AP-dependent, but not AP-independent IPSCs (Southan *et al.* 2000; Lupica *et al.* 2001). This difference may be explained by differential location of I_h channels, which may be close to release sites in BCs, but at remote locations in other interneuron types.

The simplest interpretation of the reduction in mIPSC frequency is that presynaptic I_h exerts a tonic depolarizing influence in inhibitory terminals, and that block of I_h inhibits transmitter release via hyperpolarization. This hypothesis is further supported by the observation that increasing the external K^+ concentration from 2.5 to 5 mM reverses the effect of ZD 7288 on mIPSCs (Y. Aponte, unpublished observations). How changes in membrane potential are converted into changes in frequency of mIPSCs is unknown. One possibility is that depolarization by HCN channels activates a small fraction of high-threshold Ca^{2+} channels in presynaptic terminals. In the calyx of Held, subthreshold depolarization activates a proportion of presynaptic P/Q-type Ca^{2+} channels sufficient to facilitate transmitter release (Awatramani *et al.* 2005). As synaptic transmission at BC–granule cell synapses is also mediated by P/Q-type Ca^{2+} channels (Hefft & Jonas, 2005), a similar mechanism may operate at BC output synapses. Alternatively, depolarization by HCN channels could activate low-threshold (i.e. T-type) Ca^{2+} channels, or change the driving force for electrogenic Na^+–Ca^{2+} exchanges. However, we cannot exclude the possibility that I_h is directly coupled to the release machinery, as proposed at the crayfish neuromuscular junction (Beaumont & Zucker, 2000).

Role of HCN channels for rhythmogenesis in interneuron networks

I_h channels are thought to be involved in rhythmogenesis (Pape, 1996). In particular, their role in the generation of thalamic spindle oscillations is well established (Wang & Rinzel, 1993; Pape, 1996). Fast-spiking BCs in the hippocampus *in vivo* also generate APs rhythmically, firing gamma-frequency bursts of spikes in a theta-modulated manner (Penttonen *et al.* 1998). Can I_h promote the generation of nested theta–gamma activity in networks of hippocampal BCs? The maximal activation time constant of I_h in fast-spiking BCs is ~330 ms, which after consideration of temperature differences would roughly correspond to the upper theta-frequency band. Thus, I_h channels could amplify theta oscillations driven by external septal and entorhinal inputs (Hu *et al.* 2002; Rotstein *et al.* 2005). Furthermore, I_h would be a source of tonic excitatory drive necessary for the emergence of gamma oscillations in interneuron networks (Wang & Buzsáki, 1996). Unlike tonic excitatory drive generated by metabotropic or kainate-type glutamate receptors, the drive mediated by I_h has self-regulatory properties. The activation level of I_h will be higher in interneurons that receive a small drive via other sources than in cells that receive a large drive. Thus, I_h will have a homogenizing effect on the firing frequency of interneurons, which could contribute the stability of coherent gamma oscillations in heterogeneous interneuron networks (Vida *et al.* 2006).

References

Awatramani GB, Price GD & Trussell LO (2005). Modulation of transmitter release by presynaptic resting potential and background calcium levels. *Neuron* **48**, 109–121.

Baker M, Bostock H, Grafe P & Martius P (1987). Function and distribution of three types of rectifying channel in rat spinal root myelinated axons. *J Physiol* **383**, 45–67.

Bartos M, Vida I, Frotscher M, Meyer A, Monyer H, Geiger JRP & Jonas P (2002). Fast synaptic inhibition promotes synchronized gamma oscillations in hippocampal interneuron networks. *Proc Natl Acad Sci U S A* **99**, 13222–13227.

Beaumont V & Zucker RS (2000). Enhancement of synaptic transmission by cyclic AMP modulation of presynaptic I_h channels. *Nat Neurosci* **3**, 133–141.

Buhl EH, Halasy K & Somogyi P (1994). Diverse sources of hippocampal unitary inhibitory postsynaptic potentials and the number of synaptic release sites. *Nature* **368**, 823–828.

Buzsáki G & Draguhn A (2004). Neuronal oscillations in cortical networks. *Science* **304**, 1926–1929.

Chen C (2004). ZD7288 inhibits postsynaptic glutamate receptor-mediated responses at hippocampal perforant path-granule cell synapses. *Eur J Neurosci* **19**, 643–649.

Chen S, Wang J & Siegelbaum SA (2001). Properties of hyperpolarization-activated pacemaker current defined by coassembly of HCN1 and HCN2 subunits and basal modulation by cyclic nucleotide. *J Gen Physiol* **117**, 491–503.

Chevaleyre V & Castillo PE (2002). Assessing the role of Ih channels in synaptic transmission and mossy fiber LTP. *Proc Natl Acad Sci U S A* **99**, 9538–9543.

Clements JD & Bekkers JM (1997). Detection of spontaneous synaptic events with an optimally scaled template. *Biophys J* **73**, 220–229.

Cuttle MF, Rusznák Z, Wong AYC, Owens S & Forsythe ID (2001). Modulation of a presynaptic hyperpolarization-activated cationic current (I_h) at an excitatory synaptic terminal in the rat auditory brainstem. *J Physiol* **534**, 733–744.

Day M, Carr DB, Ulrich S, Ilijic E, Tkatch T & Surmeier DJ (2005). Dendritic excitability of mouse frontal cortex pyramidal neurons is shaped by the interaction among HCN, Kir2, and K_{leak} channels. *J Neurosci* **25**, 8776–8787.

Debanne D (2004). Information processing in the axon. *Nat Rev Neurosci* **5**, 304–316.

DiFrancesco D (1981). A study of the ionic nature of the pace-maker current in calf Purkinje fibres. *J Physiol* **314**, 377–393.

Franz O, Liss B, Neu A & Roeper J (2000). Single-cell mRNA expression of *HCN1* correlates with a fast gating phenotype of hyperpolarization-activated cyclic nucleotide-gated ion channels (Ih) in central neurons. *Eur J Neurosci* **12**, 2685–2693.

Freund TF & Buzsáki G (1996). Interneurons of the hippocampus. *Hippocampus* **6**, 347–470.

Fricker D, Verheugen JA & Miles R (1999). Cell-attached measurements of the firing threshold of rat hippocampal neurones. *J Physiol* **517**, 791–804.

Gauss R, Seifert R & Kaupp UB (1998). Molecular identification of a hyperpolarization-activated channel in sea urchin sperm. *Nature* **393**, 583–587.

Geiger JRP, Lübke J, Roth A, Frotscher M & Jonas P (1997). Submillisecond AMPA receptor-mediated signaling at a principal neuron-interneuron synapse. *Neuron* **18**, 1009–1023.

Goldstein SA, Bockenhauer D, O'Kelly I & Zilberberg N (2001). Potassium leak channels and the KCNK family of two-P-domain subunits. *Nat Rev Neurosci* **2**, 175–184.

Harris NC & Constanti A (1995). Mechanism of block by ZD 7288 of the hyperpolarization-activated inward rectifying current in guinea pig substantia nigra neurons in vitro. *J Neurophysiol* **74**, 2366–2378.

Hefft S & Jonas P (2005). Asynchronous GABA release generates long-lasting inhibition at a hippocampal interneuron-principal neuron synapse. *Nat Neurosci* **8**, 1319–1328.

Hille B (2001). *Ion Channels of Excitable Membranes*. Sinauer, Sunderland, MA, USA.

Hu H, Vervaeke K & Storm JF (2002). Two forms of electrical resonance at theta frequencies, generated by M-current, h-current and persistent Na^+ current in rat hippocampal pyramidal cells. *J Physiol* **545**, 783–805.

Jonas P (1995). Fast application of agonists to isolated membrane patches. In *Single-Channel Recording*, 2nd edn, ed. Sakmann B & Neher E, pp. 231–243. Plenum Press, New York, USA.

Jonas P, Bischofberger J, Fricker D & Miles R (2004). Interneuron Diversity series: Fast in, fast out – temporal and spatial signal processing in hippocampal interneurons. *Trends Neurosci* **27**, 30–40.

Jonas P, Major G & Sakmann B (1993). Quantal components of unitary EPSCs at the mossy fibre synapse on CA3 pyramidal cells of rat hippocampus. *J Physiol* **472**, 615–663.

Lien CC, Martina M, Schultz JH, Ehmke H & Jonas P (2002). Gating, modulation and subunit composition of voltage-gated K^+ channels in dendritic inhibitory interneurones of rat hippocampus. *J Physiol* **538**, 405–419.

Liss B (2002). Improved quantitative real-time RT-PCR for expression profiling of individual cells. *Nucleic Acids Res* **30**, e89.

Lübke J, Frotscher M & Spruston N (1998). Specialized electrophysiological properties of anatomically identified neurons in the hilar region of the rat fascia dentata. *J Neurophysiol* **79**, 1518–1534.

Ludwig A, Zong X, Jeglitsch M, Hofmann F & Biel M (1998). A family of hyperpolarization-activated mammalian cation channels. *Nature* **393**, 587–591.

Lupica CR, Bell JA, Hoffman AF & Watson PL (2001). Contribution of the hyperpolarization-activated current (I_h) to membrane potential and GABA release in hippocampal interneurons. *J Neurophysiol* **86**, 261–268.

Maccaferri G & McBain CJ (1996). The hyperpolarization-activated current (I_h) and its contribution to pacemaker activity in rat CA1 hippocampal stratum oriens-alveus interneurones. *J Physiol* **497**, 119–130.

Maccaferri G, Mangoni M, Lazzari A & DiFrancesco D (1993). Properties of the hyperpolarization-activated current in rat hippocampal CA1 pyramidal cells. *J Neurophysiol* **69**, 2129–2136.

McCormick DA & Pape HC (1990). Properties of a hyperpolarization-activated cation current and its role in rhythmic oscillation in thalamic relay neurones. *J Physiol* **431**, 291–318.

Macri V & Accili EA (2004). Structural elements of instantaneous and slow gating in hyperpolarization-activated cyclic nucleotide-gated channels. *J Biol Chem* **279**, 16832–16846.

Magee JC (1999). Dendritic I_h normalizes temporal summation in hippocampal CA1 neurons. *Nat Neurosci* **2**, 508–514.

Martina M & Jonas P (1997). Functional differences in Na^+ channel gating between fast-spiking interneurones and principal neurones of rat hippocampus. *J Physiol* **505**, 593–603.

Martina M, Schultz JH, Ehmke H, Monyer H & Jonas P (1998). Functional and molecular differences between voltage-gated K^+ channels of fast-spiking interneurons and pyramidal neurons of rat hippocampus. *J Neurosci* **18**, 8111–8125.

Mellor J, Nicoll RA & Schmitz D (2002). Mediation of hippocampal mossy fiber long-term potentiation by presynaptic I_h channels. *Science* **295**, 143–147.

Monyer H & Jonas P (1995). Polymerase chain reaction analysis of ion channel expression in single neurons of brain slices. *Single-Channel Recording*, 2nd edn, ed. Sakmann B & Neher E, pp. 357–373. Plenum Press, NY, USA.

Mott DD, Turner DA, Okazaki MM & Lewis DV (1997). Interneurons of the dentate-hilus border of the rat dentate gyrus: morphological and electrophysiological heterogeneity. *J Neurosci* **17**, 3990–4005.

Notomi T & Shigemoto R (2004). Immunohistochemical localization of I_h channel subunits, HCN1-4, in the rat brain. *J Comp Neurol* **471**, 241–276.

Pape HC (1996). Queer current and pacemaker: the hyperpolarization-activated cation current in neurons. *Annu Rev Physiol* **58**, 299–327.

Penttonen M, Kamondi A, Acsády L & Buzsáki G (1998). Gamma frequency oscillation in the hippocampus of the rat: intracellular analysis *in vivo*. *Eur J Neurosci* **10**, 718–728.

Pouille F & Scanziani M (2004). Routing of spike series by dynamic circuits in the hippocampus. *Nature* **429**, 717–723.

Proenza C & Yellen G (2006). Distinct populations of HCN pacemaker channels produce voltage-dependent and voltage-independent currents. *J Gen Physiol* **127**, 183–190.

Robinson RB & Siegelbaum SA (2003). Hyperpolarization-activated cation currents: from molecules to physiological function. *Annu Rev Physiol* **65**, 453–480.

Rodrigues ARA & Oertel D (2006). Hyperpolarization-activated currents regulate excitability in stellate cells of the mammalian ventral cochlear nucleus. *J Neurophysiol* **95**, 76–87.

Rotstein HG, Pervouchine DD, Acker CD, Gillies MJ, White JA, Buhl EH, Whittington MA & Kopell N (2005). Slow and fast inhibition and an H-current interact to create a theta rhythm in a model of CA1 interneuron network. *J Neurophysiol* **94**, 1509–1518.

Rudy B & McBain CJ (2001). Kv3 channels: voltage-gated K^+ channels designed for high-frequency repetitive firing. *Trends Neurosci* **24**, 517–526.

Santoro B, Chen S, Lüthi A, Pavlidis P, Shumyatsky GP, Tibbs GR & Siegelbaum SA (2000). Molecular and functional heterogeneity of hyperpolarization-activated pacemaker channels in the mouse CNS. *J Neurosci* **20**, 5264–5275.

Santoro B, Liu DT, Yao H, Bartsch D, Kandel ER, Siegelbaum SA & Tibbs GR (1998). Identification of a gene encoding a hyperpolarization-activated pacemaker channel of brain. *Cell* **93**, 717–729.

Soleng AF, Chiu K & Raastad M (2003). Unmyelinated axons in the rat hippocampus hyperpolarize and activate an H current when spike frequency exceeds 1 Hz. *J Physiol* **552**, 459–470.

Soltesz I, Smetters DK & Mody I (1995). Tonic inhibition originates from synapses close to the soma. *Neuron* **14**, 1273–1283.

Southan AP, Morris NP, Stephens GJ & Robertson B (2000). Hyperpolarization-activated currents in presynaptic terminals of mouse cerebellar basket cells. *J Physiol* **526**, 91–97.

Vasilyev DV & Barish ME (2002). Postnatal development of the hyperpolarization-activated excitatory current I_h in mouse hippocampal pyramidal neurons. *J Neurosci* **22**, 8992–9004.

Vida I, Bartos M & Jonas P (2006). Shunting inhibition improves robustness of gamma oscillations in hippocampal interneuron networks by homogenizing firing rates. *Neuron* **49**, 107–117.

Wang X-J & Buzsáki G (1996). Gamma oscillation by synaptic inhibition in a hippocampal interneuronal network model. *J Neurosci* **16**, 6402–6413.

Wang X-J & Rinzel J (1993). Spindle rhythmicity in the reticularis thalami nucleus: synchronization among mutually inhibitory neurons. *Neuroscience* **53**, 899–904.

Williams SR & Stuart GJ (2000). Site independence of EPSP time course is mediated by dendritic I_h in neocortical pyramidal neurons. *J Neurophysiol* **83**, 3177–3182.

Wollmuth LP & Hille B (1992). Ionic selectivity of I_h channels of rod photoreceptors in tiger salamanders. *J Gen Physiol* **100**, 749–765.

Yamada R, Kuba H, Ishii TM & Ohmori H (2005). Hyperpolarization-activated cyclic nucleotide-gated cation channels regulate auditory coincidence detection in nucleus laminaris of the chick. *J Neurosci* **25**, 8867–8877.

Acknowledgements

We thank Drs J. Bischofberger and B. Fakler for critically reading the manuscript and S. Becherer, M. Northemann and K. Winterhalter for technical assistance. Supported by Deutsche Forschungsgemeinschaft grants to P.J. (Sonder forschūngsbereich 505/C5 and Graduiertenkolleg 843).

Author's present address

C.-C. Lien: University of California, Berkeley, Department of Molecular and Cell Biology, Berkeley, CA, USA.

Hyperpolarization-activated cation channels in fast-spiking interneurons of rat hippocampus

Yexica Aponte, Cheng-Chang Lien, Ellen Reisinger and Peter Jonas

J. Physiol. 2006;574;229-243; originally published online May 11, 2006;

DOI: 10.1113/jphysiol.2005.104042